

Current-Driven Switching in Magnetic Multilayer Nanopillars

S. Urazhdin, Norman O. Birge, W. P. Pratt Jr., and J. Bass

Department of Physics and Astronomy, Center for Fundamental Materials Research and Center for Sensor Materials, Michigan State University, East Lansing, MI 48824

We summarize our recent findings on how the current-driven magnetization switching in nanofabricated magnetic multilayers is affected by an applied magnetic field, changes of temperature, magnetic coupling between the ferromagnetic layers, variations in the multilayer structure, and the relative rotation of the layers' magnetizations. We show how these results can be interpreted with a model describing current-driven excitations as an effective current-dependent magnetic temperature.

I. INTRODUCTION

An exchange-based mechanism for current-driven switching of magnetization was predicted by Slonczweski [1] and Berger, [2] and later observed experimentally. [3, 4] Recent research has been directed towards better understanding of the current-driven excitation mechanism, adequate description of the magnetic dynamics, and optimization of magnetic devices e.g. to decrease the switching current I_s for possible applications in magnetic memory. [5, 6, 7, 8, 9, 10, 11, 12, 13, 14, 15, 16, 17, 18, 19, 20, 21, 22, 23, 24, 25, 26, 27, 28, 29, 30, 31, 32]

We used the giant magnetoresistance effect (MR) to study current-driven switching in nanofabricated magnetic $F_1/N/F_2$ trilayers (nanopillars). We studied how the current-driven switching is affected by variations of the magnetic field H , ambient temperature T_{ph} , [25] coupling between magnetic layers, [24, 30] electron spin-flipping in the spacer N or outside the trilayer, and mutual rotation of the two layers' magnetizations [31]. We interpret our experimental results for currents that are not too large in terms of the recently proposed effective temperature model. [32]

Our samples were made with a multistep process described elsewhere. [24] Below, all thicknesses are in nm. The basic samples had structure $Cu(80)/F_1(20-30)/N(10-15)/F_2(2-6)/Cu(2-5)/Au(150)$. F was either Co or $Py=Ni_{84}Fe_{16}$. Although Co is commonly used in studies of current-driven switching, Py has the advantage of small crystalline anisotropy and magnetostriction, allowing reproducible measurements at both 295 K and 4.2 K. The bottom $Cu(80)$ layer was the extended lead, N , F_2 and $Cu(2-5)$ were patterned into an elongated shape with dimensions $\approx (130 - 140) \times (60 - 70) \text{ nm}^2$, and $Au(150)$ was the top lead. In all the samples, except for the AF-coupled ones (see Section. III), F_1 was left extended to minimize the effect of dipolar coupling on the current-driven switching. [11] Details of specific samples will be given with their data. We measured dV/dI with four-probes and lock-in detection, adding an ac current of amplitude 20–40 μA at 8 kHz to the dc current I . Positive current flows from F_1 to F_2 . H is in the film plane and (except for the angular dependence studies) along the nanopillar easy axis.

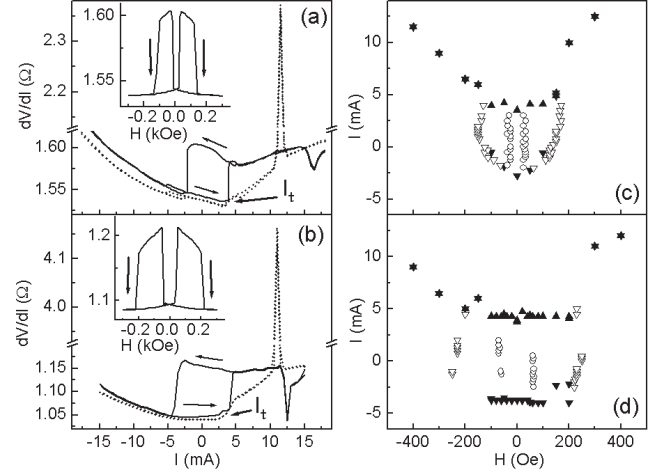


FIG. 1: (a) Switching with current at 295 K in an uncoupled Py/Cu/Py trilayer. Solid line: $H = 50$ Oe, dashed line: $H = -500$ Oe. Arrows mark the scan direction. I_t is the threshold current as defined in the text. Inset: MR dependence on H at $I = 0$. (b) Same as (a), at 4.2 K. (c),(d) Magnetization switching diagram, extracted from the current-switching at fixed H (solid symbols), and field-switching at fixed I (open symbols): (c) at 295 K, (d) at 4.2 K. Downward triangles: AP to P switching, upward: P to AP switching, circles: switching of the extended Py(20) layer. The reversible switching peaks are marked by coinciding upward and downward triangles. From Urazhdin *et al.* [25]

II. SWITCHING WITH VARIED H AND T_{ph}

Figs. 1(a,b) and insets show the variations of dV/dI with I and H for a $Py(20)/Cu(10)/Py(6)$ sample with uncoupled Py layers at 295 K (1a) and 4.2 K (1b), for $H = 50$ Oe (solid curves) and $H = 500$ Oe (dashed curves). The dependencies are similar to those seen in Co/Cu/Co samples. [11, 24] At small H , the magnetization switches hysteretically to a higher resistance AP state at a large enough positive current $I_s^{P \rightarrow AP} \equiv I_s > 0$, and to a low resistance P state at $I_s^{AP \rightarrow P} < 0$. At larger H , the switching step turns into a, often much higher, nonhysteretic peak. The asymmetric I -dependence is a signature of the effect of the current on the magnetization, different from the Oersted field. Figs. 1(c,d) show the switching diagrams at 295 K and 4.2 K, extracted from data such as those in Figs. 1(a,b), obtained both

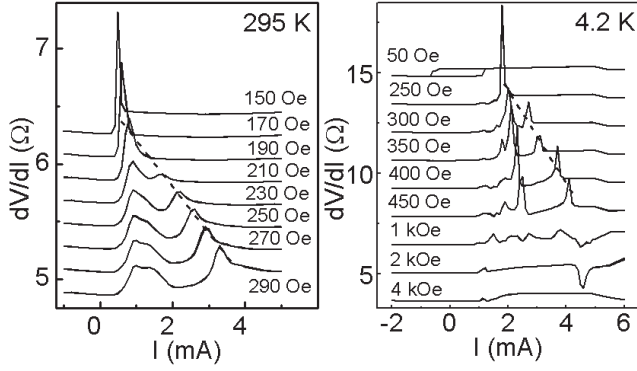


FIG. 2: Differential resistance of a Py(20)/Cu(10)/Py(3.5) uncoupled trilayer at the marked values of H , at 295 K (left) and 4.2 K (right). Curves are offset for clarity. Dashed lines follow the reversible switching peak.

by varying I at fixed H and H at fixed I . As expected, both the reduced magnetization and thermal activation result in smaller switching currents and fields $H_s(I=0)$ at 295 K. The only other major difference between the 295 K and 4.2 K data in Figs. 1(a,c) is the rounding of the 295 K hysteretic region at $I < 0$. In contrast, the hysteretic region at 4.2 K (Fig. 1(d)) is almost square.

In the reversible switching regime, both the 295 K and 4.2 K current-dependencies in Fig. 1 show a nearly linear rise of dV/dI above a threshold current I_t (labeled in Figs. 1(a,b)). In some samples, this rise displays structures, clearly distinguishable from the switching peak due to their very weak dependence on H . Fig. 2 shows data for a small Py(20)/Cu(10)/Py(3.5) sample, with dimensions estimated at $50 \times 100 \text{ nm}^2$. At 4.2 K, the linear rise is resolved into several peaks. They appear only to the left of the reversible switching peak, as the latter moves to higher I with increasing H (shown by a dashed line). At 295 K, the peaks are replaced by a smeared non-monotonic structure in dV/dI . Based on the data shown in Figs. 1 and 2, and 9 other similar Py/Cu/Py samples studied, [25] we summarize the aspects of the threshold behavior: i) I_t is close to the small- H value of $I_s^{P \rightarrow AP}$ at 4.2 K. The correspondence $I_s \approx I_t$ is not universal, e.g. in magnetically coupled samples the switching may occur at $I < 0$ (see Section III). ii) Both I_t and the sometimes observed structures in dV/dI at $I > I_t$ are only weakly dependent on H , as compared to the reversible switching peak. The 4.2 K data in Fig. 2 for $H = 4 \text{ kOe}$ give $I_t \approx 1.0 \text{ mA}$, only 25% larger than $I_t \approx 0.8 \text{ mA}$ at 250 Oe. iii) The height and inverse width of the reversible switching peak in dV/dI are correlated with the structure in dV/dI at $I > I_t$: for example, in Fig. 2 (the 295 K data), the reversible peak is tall and narrow when it is on the rising slope of the 'hump', but becomes wide and nearly disappears when on the trailing slope.

We discuss first the nature of the threshold behavior starting at I_t , and then the reversible switching peak at higher I . I_t has been identified as the onset of large amplitude excitation of the patterned Py layer, as the

magnetic energy provided by the current exceeds the linear magnetic damping rate. [25] Starting at I_t , there is a strong increase of excitation amplitude, and the highly excited magnetic state is manifested by increases in dV/dI , as illustrated in Figs. 1, 2. In all of our Co/Cu/Co samples, and most of our Py/Cu/Py samples, the excitations result in a nearly linear increase in dV/dI above I_t (see Fig. 1, and high H curves in Fig. 4(b)). In contrast, in Py/Cu/Py samples with small lateral dimensions, at 4.2 K the excitations appear as a series of peaks in dV/dI above I_t (Fig. 2), corresponding to step increases in resistance V/I , with details that vary from sample to sample. We attribute these peaks to irregularities in sample shapes, resulting in a complicated dependence on I of both the magnetic damping rates and the distribution of excitations among different magnetic modes. In larger samples, the shape irregularities are less significant, giving a smoother dV/dI .

A different, quantum-mechanical origin has been proposed for the peaks, interpreted as the excitation threshold in point-contacts on magnetic multilayers. [3] This threshold would be due to the requirement for matching of the current-driven spin-accumulation with the lowest energies of the magnetic excitations, $\Delta\mu = \hbar\omega$. In nanopillars, the quantum threshold value would double when H is increased from 0 to $\approx 1 \text{ kOe}$. Such a rapid increase is inconsistent with our data. In addition, even at 4.2 K, thermal smearing with $kT_{ph} \gg \hbar\omega \approx 10 \text{ } \mu\text{eV}$ would completely smear out the quantum threshold. Thus, experiments rule out the quantum nature of the excitation threshold in nanopillars. We note that at large $H > 2\pi M \approx 5 \text{ kOe}$, both the classical and quantum-mechanical thresholds depend linearly on H , and $\hbar\omega$ may become comparable to kT . In this limit, the quantum threshold may become important.

The reversible switching peak in dV/dI is different from the threshold I_t and the peaks we associate with magnetic excitations. Time resolved measurements showed that it is a consequence of telegraph noise with random distribution of dwell times in the P and AP states. [24, 25] Fig. 3(a) shows the variations of average dwell times $\tau_P(\tau_{AP})$ in the P(AP) state with I for a Py(20)/Cu(10)/Py(6) sample at 295 K and 4.2 K. τ_P decreases as I increases, but τ_{AP} increases. These variations have a similar form at 295 K and 4.2 K, and are also similar to the variations in Co/Cu/Co. [13] Fig. 3(b) shows that at a fixed I , τ_P increases and τ_{AP} decreases as $|H|$ is increased (shown for 295 K). Fig. 3(c) shows that, when both I and H are increased so as to hold $\tau_P = \tau_{AP}$, the average period of the telegraph noise decreases exponentially with similar slopes at 295 K and 4.2 K, down to the 1 MHz bandwidth limit of our setup.

We now show how a peak in dV/dI at $\tau_P \approx \tau_{AP}$ can be derived from the variations of τ_P, τ_{AP} with I . For a fixed H , the average voltage across the sample is

$$V(I) = I \left[\frac{R_{AP}\tau_{AP} + R_P\tau_P}{\tau_P + \tau_{AP}} \right], \quad (1)$$

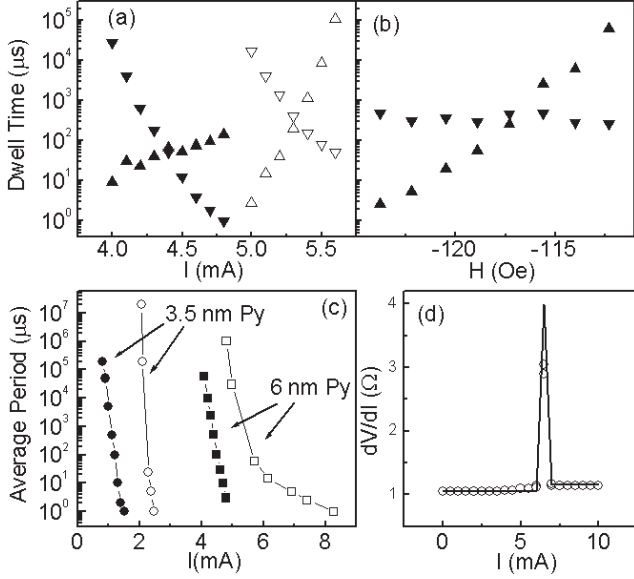


FIG. 3: (a) The dependence of the P (downward triangles) and AP (upward triangles) dwell times on I , for a Py(20)/Cu(10)/Py(6) uncoupled sample. Open symbols: $T_{ph} = 4.2$ K, $H = -335$ Oe, filled symbols: $T_{ph} = 295$ K, $H = -120$ Oe. (b) Dependence of P (downward triangles) and AP (upward triangles) dwell times on H at $I = 4.4$ mA, $T = 295$ K. (c) Current dependence of the average telegraph noise period. H was adjusted approximately linearly with I , so that the average dwell times in AP and P states were equal. Solid circles: Py(20)/Cu(10)/Py(3.5) at 295 K, $H = 93$ to -121 Oe, open circles: same sample at 4.2 K, $H = -300$ to -315 Oe, solid squares: Py(20)/Cu(10)/Py(6) at 295 K, $H = -113$ to -123 Oe, open squares: same sample at 4.2 K, $H = -300$ to -450 Oe. (d) Circles: dV/dI vs. I at $H = -0.3$ kOe, 4.2 K. Solid curve: a calculation, as described in the text, with $I_0 = 6.45$ mA, and $\alpha + \beta = 27$ mA $^{-1}$ obtained from (a).

with $\tau_P(I) \approx \tau_0 \exp[-\alpha(I - I_0)]$, $\tau_{AP}(I) \approx \tau_0 \exp[\beta(I - I_0)]$, as in Fig. 3(a). We define I_0 , τ_0 by $\tau_{AP}(I_0) = \tau_P(I_0) = \tau_0$. From Eq. (1)

$$dV/dI \approx R_P + \frac{R_{AP} - R_P}{1 + \exp[-(\alpha + \beta)(I - I_0)]} + I(R_{AP} - R_P) \frac{\exp[(\alpha + \beta)(I - I_0)](\alpha + \beta)}{(\exp[(\alpha + \beta)(I - I_0)] + 1)^2}. \quad (2)$$

The first two terms on the right are the resistance V/I , giving a step for the reversible transition from P to AP. For large $I_0(\alpha + \beta)$, the last term has a maximum value $I_0(R_{AP} - R_R)(\alpha + \beta)/4$ at $I \approx I_0$. This term gives rise to a peak in dV/dI at $I = I_0$ that can be much higher than R_{AP} . Fig. 3(d) shows a calculation (solid line) based on the data of Fig. 3(a), and Eq. (2), for $I_0 = 6.45$ mA, and $\alpha + \beta = 27$ mA $^{-1}$ extracted from fig. 3(a). The calculation is consistent with the dV/dI measurement (circles). We conclude that the reversible switching peak positions characterize the points (H, I) where $\tau_P = \tau_{AP}$. The slope of the reversible switching line is a measure of the telegraph noise variation with I, H . From Eq. 2, the height

and inverse width of the reversible switching peak are given by $\alpha + \beta$, which is usually dominated by α , i.e. the dependence of the magnetic excitation rate in the P state on I . This is consistent with the correlation in Fig. 2(a) between the reversible switching peak and the 'bump' associated with magnetic excitations: On the positive slope of the 'bump' ($H = 150, 170$ Oe), the excitation level grows faster with I than on its trailing slope. Consequently, α is larger on the rising slope of the bump, giving a tall and narrow reversible switching peak. The reversible peak nearly disappears on the trailing slope at $H = 190, 210$ Oe, where α is small.

In contrast to I_t , the switching peak does not represent an onset of a physical process, it merely reflects the current-dependent telegraph noise statistics. The presence of telegraph noise near the reversible switching line indicates that both AP and P states are unstable there. Strictly, the stability diagrams, Figs. 1(c,d) should be modified to include this unstable region. In most uncoupled samples, the P-state becomes unstable at $I \approx I_t$. The instability of the P-state at $I > I_t$ is thus indirectly manifested in the rise of R_P . The AP-state is unstable at I both below and above the reversible switching peak. Since τ_P is exponentially smaller than τ_{AP} , the measurements of dV/dI at I above the reversible switching peak give values very near R_{AP} .

As I and H are increased, τ_P, τ_{AP} quickly approach the intrinsic nanosecond switching timescale (see Fig. 3(c)), where telegraph noise is replaced by some sort of fast magnetic dynamics. Such a transition does not give any significant changes in the switching peaks in dV/dI (see e.g. Fig. 2). Although the bandwidth limitation of our setup does not allow us to directly probe this regime, spectroscopic measurements show continuous spectrum from 0 Hz up to ≈ 1 MHz, characteristic of incoherent magnetic dynamics. [33] Microwave measurements show peaks at GHz frequencies on top of a broad background, evidence for some level of coherence. [28]

III. EFFECTS OF MAGNETIC COUPLING

Fig. 4 summarizes the differences between uncoupled (left), AF-coupled (middle), and F-coupled (right) Co(20)/Cu(d)/Co(2.5) samples at 295 K. For uncoupled samples, we used $d=10$, and only patterned the top Co(2.5) and most of the Cu(10) layer to nanopillar size, leaving the bottom Co(20)-layer extended. F coupling was achieved by reducing the Cu thickness to Cu(2.6), near the third RKKY magnetoresistance (MR) minimum. [36] Dipolar AF coupling was achieved by also patterning about 10 nm of the Co(20) layer, with $d = 6$. Sample shape variations and interfacial roughness lead to variations in both AF and F coupling strengths.

Fig. 4(a)) shows field-driven switching in uncoupled samples, similar to that in Fig. 1 for uncoupled Py-based samples. In AF-coupled samples (Fig. 4(d)), the Co(2.5) layer is oriented AP to the extended Co(20) layer by the

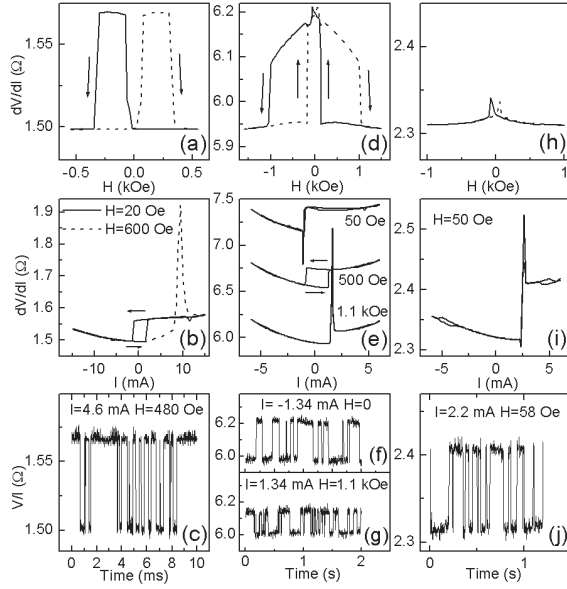


FIG. 4: Results for uncoupled (a-c), AF-coupled (d-g), and F-coupled (h-j) Co/Cu/Co samples at 295 K. In the hysteretic plots, arrows show the scan direction. (a,d,h) dV/dI vs. H at $I = 0$. (b,e,i) dV/dI vs. I at the listed values of H . In (e) curves are offset for clarity. (c,f,g,j) Time-resolved measurements of $R=V/I$ at the listed values of H , I . From Ref. [30]

dipolar field, so only the high resistance AP state is stable at $H = 0$. In contrast to Fig. 4(a), both the $P \rightarrow AP$ and $AP \rightarrow P$ transitions are now due to switching of the Co(2.5) layer. As H is scanned from a large negative to a large positive value, this layer switches three times: once to the AP state at negative H , then together with the Co(20) layer at small positive H to stay in the AP state, and finally to a P state at large positive H . The second transition sometimes produces a weak feature in dV/dI . In contrast, F-coupling causes the magnetizations to reverse simultaneously at small H , giving only a small feature in MR at $I=0$ (Fig. 4(h)). In H -scans at large enough fixed $I > 0$, F-coupled samples gave 5% MR, similar to the $I = 0$ values for uncoupled or AF-coupled samples.

Fig. 4(b,e,i) compares the variations of dV/dI with I . At small $H = 20-50$ Oe, applied to fix the magnetization of the bottom Co layer, the uncoupled sample (Fig. 4(b), solid curve) shows hysteretic switching, while the AF-coupled (Fig. 4(e), top curve) and F-coupled (Fig. 4(i)) ones show reversible switching at $I < 0$ and $I > 0$, respectively. At larger H , the switching in uncoupled samples (Fig. 4(b), dashed curve) becomes reversible, and in AF-coupled samples (Fig. 4(e), lower two curves) it first becomes hysteretic and then reversible again. Time resolved measurements of resistance at I, H near the reversible switching peaks show telegraph noise switching between AP and P states (Fig. 4(c,f,g,j)). At identical I of opposite signs, the average telegraph noise periods in the AF-coupled sample are similar.

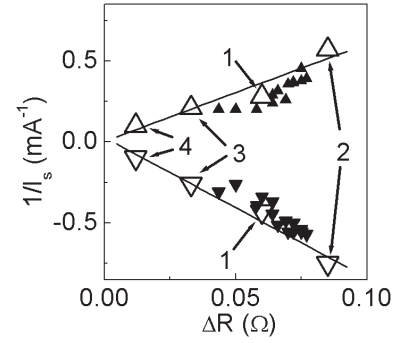


FIG. 5: Dependence of $1/I_s^{P \rightarrow AP}$ (upward triangles) and $1/I_s^{AP \rightarrow P}$ (downward triangles) on ΔR for uncoupled samples. Open symbols: sample types 1 through 4, as labeled and explained in the text. Solid lines: best linear fits of data, excluding the angular dependence. The ordinate intercepts are zero within the uncertainty of the fits.

IV. RELATION BETWEEN MR AND I_s

We studied the correlation between MR and I_s in uncoupled samples with a structure Cu(80)/Py(30)/N(15)/Py(6)/Cu(2)/Au(150). $N=Cu$ in sample types 1 and 2. In sample types 3 and 4, N was Cu(9.5)/Cu₉₄Pt₆(4)/Cu(1.5) and Cu(5.5)/Cu₉₄Pt₆(8)/Cu(1.5), respectively. The short 295 K spin-diffusion length $t_{sf} \approx 6$ nm (≈ 9 nm at 4.2 K [35]) in Cu₉₆Pt₆ decreases $\Delta R \equiv R_{AP} - R_P$. We enhanced ΔR in sample type 2 by replacing Cu(2) with a Cu(2)/Fe₅₀Mn₅₀(1)/Cu(2) sandwich. Fe₅₀Mn₅₀ is a strong spin-scatterer. [35] Its placement between the trilayer and the top lead reduces the negative effect of the spin accumulation outside the trilayer on the MR. We also examined the variation of ΔR and the switching currents I_s in samples of type 1 while rotating the magnetization of the Py(30) with a small H in the film plane (similar results were shown in [26]).

The results, averaged over at least 7 samples of each type, are summarized in Fig. 5, where data for angular dependence are also shown. Both I_s^{AP} and I_s^{AP} follow an approximately inversely linear dependence on ΔR , regardless of the method by which ΔR was varied.

V. EFFECTIVE TEMPERATURE MODEL

In their pioneering work, Slonczewski [1] and Berger, [2] predicted that exchange interaction leads to current-driven magnetic excitation by spin-polarized current. Berger considered generation of magnons by spin-flipping of electrons, driven by the spin accumulation. Slonczewski considered the electron spin component transverse to the magnetization, which is absorbed by the ferromagnet due to a combination of spin-dependent reflection at the interfaces and averaging of the spin precession phases in the ferromagnet. The re-

sulting torque drives the magnetic dynamics. This model postulates conservation of the total magnetic moment, and thus captures only the coherent (uniform) magnetic dynamics. It can not consistently treat the excitation of finite-wavelength spin-waves, whose generation is generally not associated with transfer of angular momentum transverse to the magnetization (a similar argument is used to prove that only uniform precession is excited in the transverse FMR experiments). Similarly, Berger made the approximation that only the uniform precession is generated by electron spin-flipping, leading again to coherent magnetic dynamics.

Since the characteristic magnon energies are significantly lower than the typical conduction electron energies (see the above discussion of the lack of quantum threshold behavior), we assume that a large number of magnetic modes are excited by the current. The populations n_i of the modes with energies E_i can be then approximately described by a single parameter, an effective temperature T_m , so that $n_i \approx k_B T_m / E_i$ for the degenerate modes. [24, 25, 32] This approximation fails when T_m approaches the Curie temperature of the ferromagnet. We emphasize that this is just a single-parameter approximation for a generally much more complex, non-thermalized excitation distribution. Because of the large magnon populations, the spontaneous (independent of n_i) magnon emission can be neglected. In a ballistic transport approximation [32]

$$kT_m \approx \frac{kT_{ph}}{1 + 2peVB/\gamma}, \quad (3)$$

where B is a constant characterizing the strength of the exchange interaction, γ is related to the Gilbert damping parameter in the classical Landau-Lifshitz equation, V is the voltage across the trilayer, and p is the current polarization, created at the location of F_2 by F_1 , if F_2 is removed. $p > 0 (< 0)$ in the P(AP) state for Py/Cu/Py or Co/Cu/Co trilayers, and $p = 0$ if F_1 is removed. Eq. 3 is similar to the expression obtained by Berger in a diffusive transport approximation (Eq. (9) in Ref. [6]).

Eq. (3) diverges at $V \rightarrow -\gamma/(2peB)$. We identify this divergence with the threshold I_t for the large amplitude of excitations. Eq. (3) is not applicable above the threshold, because the conduction electrons are scattered with a large spin-flip probability (≈ 0.5), nearly independent of T_m . For this regime, we have proposed an empirical relation [25]

$$T_m = T_{ph} + K(I - I_t) \text{ for } I > I_t, \quad (4)$$

where K is a constant determined by the magnetic relaxation rate. In the thermal activation model, the dwell times $\tau_{P,AP}$ are determined by

$$\tau_{P,AP} = \frac{1}{\Omega} \exp \left[\frac{U_{P,AP}}{kT_m^{P,AP}} \right], \quad (5)$$

where $\Omega \approx 10^7 s^{-1}$ [34] is the effective attempt rate, $U_{P,AP}$ is the potential barrier for switching from the P or

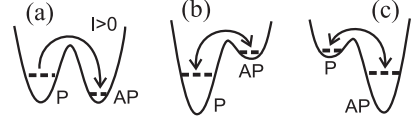


FIG. 6: Schematics of current-driven switching, as explained in the text. Dashed lines indicate T_m .

AP state. T_m is approximated by Eq. (3) for the low- H hysteretic switching, or Eq. (4) for the telegraph noise. The areas of the P(AP) state stability are determined by $\tau_{P(AP)} > 1$ s. $U_{P,AP}$ depend on I only through the variation of the magnetization with T_m .

Fig. 6(a) schematically describes hysteretic current-driven switching in uncoupled samples at small H . From Eq. (3), T_m^P drastically increases when I approaches I_t , giving rise to a thermally activated transition into the AP state at $kT_m^P \approx \frac{U_P}{\ln(t_{exp}\Omega)} \approx \frac{U_P}{16}$, for the data acquisition time $t_{exp} = 1$ sec/point. In the AP state, Eq. (3) predicts that the magnetic system weakly cools to $T_m^{AP} < T_{ph}$, so that at $H < H_s$ it becomes trapped in this state. Fig. 6(b) is a schematic for $H > H_s$, giving $kT_{ph} > \frac{U_{AP}}{16}$. The AP to P switching is now thermally activated, resulting in telegraph noise at $I > I_s$, $H > H_s$. Fig. 6(c) is the schematic for AF-coupled samples at small H . AF coupling increases U_{AP} and reduces U_P , so that P to AP switching is now thermally activated. At large enough $I < 0$, reverse switching also becomes thermally activated, giving telegraph noise. As H grows, the schematic for AF-coupling becomes 6(a), giving hysteretic switching, and then 6(b), giving telegraph noise for large enough positive I . Finally, 6(b) is the schematic for F-coupling at all H , so that AP to P switching is always thermally activated and large enough $I > 0$ gives telegraph noise.

The difference between the 295 K and 4.2 K switching diagrams (Fig. 1) is qualitatively well described by the effective temperature model. [32] The rounding of the 295 K diagram at $I < 0$ is due to enhancement of thermal fluctuations of magnetization even at small I (see Eq. 3). Increasing H decreases U_{AP} , so that even these weak excitations can activate the AP \rightarrow P transition. In contrast, the almost square 4.2 K diagram reflects the small excitation amplitude at $I < I_t$, beyond which the excitation rapidly grows, giving the switching.

We use Eqs. (4) and (5) to describe the dependencies of τ_P on I , H , and T_{ph} in Fig. 3. Eq. (3) should be used for $\tau_{AP}(I, H, T_{ph})$. These equations capture the tendencies qualitatively well. From the slope of $\tau_P(I)$, the increase rate of T_m^P in Py(20)/Cu(10)/Py(6) samples is estimated at ≈ 400 K/mA. [25] The thermal activation model breaks down when $k_B T_m$ becomes similar to U_P . This limitation of the model should be understood in the context of the actual magnetic dynamics. $T_m \approx U$ in Eq. 5 gives a switching rate similar to the intrinsic magnetic dynamic rates. Telegraph noise switching is then replaced with fast fluctuations of the magnetic moment.

The effective temperature concept (defined for a given magnetic orientation) becomes irrelevant in this regime.

We note that, although the 295 K and 4.2 K current-dependencies in Fig. 3(a) are given for different values of H , the effect of this difference on τ_P should be small, as can be seen from Fig. 3(b). Since U_P is large, its relative variation with H is small, compared to much larger relative variation of U_{AP} . Thus, Fig. 3(a) can be used to determine $\tau_P(I)$, while τ_{AP} is adjusted with H .

Finally, to describe the inverse relationship in Fig. 5, we use the simplest plausible model, in which ΔR is proportional to the current polarization p at the location of F_2 due to F_1 . This crude approach is self-consistent: the MR is correctly predicted to disappear if F_1 is absent. The current-driven switching occurs at $16k_B T_m \approx U$. From Eq. 3 follows $1/I_s \propto p$, giving the dependence in Fig. 5. In this context, the angular dependence can be understood similarly in terms of the projection of p onto the direction of the magnetization of F_2 .

VI. SUMMARY

We summarize the following important experimental observations for current effects in magnetic trilayer

nanopillars: i) a square switching diagram at 4.2 K, and rounded at 295 K; ii) an onset current I_t (closely related to the hysteretic switching current I_s) for a linear rise of dV/dI in larger samples or a series of peaks in smaller ones; iii) reversible switching, characterized by telegraph noise with rate both increasing exponentially with I and shifting with temperature. The reversible switching peak in dV/dI occurs when the dwell times in the P and AP states are approximately equal. iv) Reversible switching at small H , if magnetic layers are F- or AF-coupled. v) Inverse linear relation between MR and I_s . We explain the observed behaviors in terms of thermal activation over a magnetic barrier, with a current driven effective magnetic temperature.

We acknowledge helpful communications with M.D. Stiles, A.H. MacDonald, D.C. Ralph, S. Zhang, A. Fert, support from the MSU CFMR, CSM, the MSU Keck Microfabrication facility, the NSF through Grants DMR 02-02476, 98-09688, and NSF-EU 00-98803, and Seagate Technology.

-
- [1] J. Slonczewski, J. Magn. Magn. Mater. **159**, L1 (1996).
 - [2] L. Berger, Phys. Rev. **B 54**, 9353 (1996).
 - [3] M. Tsoi et al., Phys. Rev. Lett. **80**, 4281 (1998); **81**, 493(E) (1998).
 - [4] E.B. Myers et al., Science **285**, 867 (1999).
 - [5] J. Slonczewski, J. Magn. Magn. Mater. **195**, L261 (1999); ibid. 2473242002.
 - [6] L. Berger, Phys. Rev. **B 59**, 11465 (1999).
 - [7] X. Waintal et al., Phys. Rev. **B 62**, 12317 (2000).
 - [8] J. Z. Sun, Phys. Rev. **B 62**, 570 (2000).
 - [9] M. Tsoi et al., Nature (London) **406**, 46 (2000).
 - [10] J.A. Katine et al., Phys. Rev. Lett. **84**, 3149 (2000).
 - [11] F. J. Albert et al., Appl. Phys. Lett. **77**, 3809 (2000).
 - [12] J. Grollier et al., Appl. Phys. Lett. **78**, 3663 (2001); ibid, Phys. Rev. **B 67**, 174402 (2003).
 - [13] E. B. Myers et al., Phys. Rev. Lett. **89**, 196801 (2002).
 - [14] F. J. Albert et al., Phys. Rev. Lett. **89**, 226802 (2002).
 - [15] S. Zhang, P. M. Levy, A. Fert, Phys. Rev. Lett. **88**, 236601 (2002).
 - [16] J. E. Wegrowe et al., J. Appl. Phys. **91**, 6806 (2002).
 - [17] M. Tsoi et al., Phys. Rev. Lett. **89**, 246803 (2002).
 - [18] M. D. Stiles and A. Zangwill, J. Appl. Phys. **247**, 324 (2002), Phys. Rev. **B 66**, 014407 (2002).
 - [19] A. Kovalev, A. Brataas, and G. E. W. Bauer, Phys. Rev. **B 66**, 224424 (2002).
 - [20] J. Z. Sun et al., J. Appl. Phys. **93**, 6859 (2003).
 - [21] Y. Ji, C.L. Chien, and M.D. Stiles, Phys. Rev. Lett. **90**, 106601 (2003).
 - [22] B. Oezylmaz et al., Phys. Rev. Lett. **91**, 067203 (2003).
 - [23] A. Shpiro, P. M. Levy, S. Zhang, Phys. Rev. **B 67**, 104430 (2003).
 - [24] S. Urazhdin et al., Appl. Phys. Lett. **83**, 114 (2003).
 - [25] S. Urazhdin et al., Phys. Rev. Lett. **91**, 146803 (2003).
 - [26] F.B. Mancoff et al., Appl. Phys. Lett. **83**, 1596 (2003).
 - [27] Z. Li and S. Zhang, cond-mat/0302339.
 - [28] S.I. Kiselev et al., Nature **425**, 380 (2003).
 - [29] R.H. Koch, J.A. Katine, and J.Z. Sun, preprint.
 - [30] S. Urazhdin, W.P. Pratt Jr., J. Bass, to be published in J. Magn. Magn. Mater., cond-mat/0304299
 - [31] S. Urazhdin et al., cond-mat/0309191.
 - [32] S. Urazhdin, cond-mat/030832.
 - [33] S. Urazhdin, W.P. Pratt Jr., J. Bass, unpublished.
 - [34] R. H. Koch et al., Phys. Rev. Lett. **84**, 5419 (2000).
 - [35] W. Park et al., Phys. Rev. **B 62**, 1178 (2000).
 - [36] S.S.P. Parkin, R. Bhadra, and K.P. Roche, Phys. Rev. Lett. **66** (1991) 2152.